Science of the Total Environment 823 (2022) 153729

Contents lists available at ScienceDirect

Science of the Total Environment

journal homepage: www.elsevier.com/locate/scitotenv

# Assessing the impact of vehicular particulate matter on cultural heritage by magnetic biomonitoring at Villa Farnesina in Rome, Italy

Aldo Winkler [a,*], Tania Contardo [b], Virginia Lapenta [c], Antonio Sgamellotti [c], Stefano Loppi [b]

[a] Istituto Nazionale di Geofisica e Vulcanologia, 00143 Rome, Italy
[b] Department of Life Sciences, University of Siena, 53100 Siena, Italy
[c] Accademia Nazionale dei Lincei, 00165 Rome, Italy

## HIGHLIGHTS

- Magnetic biomonitoring methodologies were successfully applied at Villa Farnesina, Rome.
- The bioaccumulation of vehicular PM decreases with distance from a major road.
- Roadside leaves accumulate PM, providing preventive conservation services.
- Lichen transplants are suitable for investigating the diffusion of PM indoors.
- Villa Farnesina frescoed Halls are preserved from vehicular metallic emissions.

## GRAPHICAL ABSTRACT

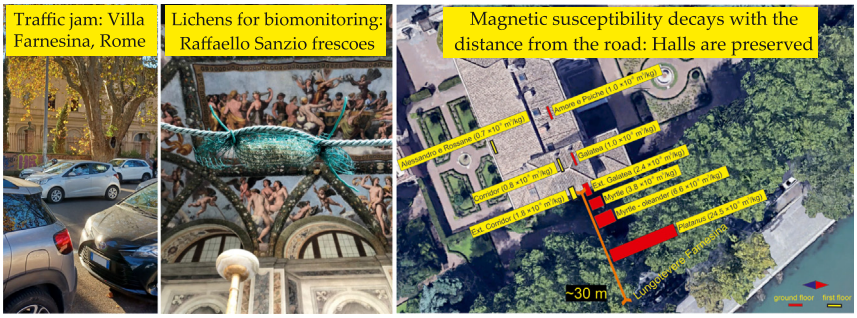


## ARTICLE INFO

*Article history:*
Received 23 December 2021
Received in revised form 3 February 2022
Accepted 3 February 2022
Available online 7 February 2022

Editor: Elena Paoletti

*Keywords:*
Magnetic biomonitoring
Traffic-related particulate matter
Lichen transplants
Brake wear
Cultural heritage
Preventive conservation

## ABSTRACT

Magnetic biomonitoring methodologies were applied at Villa Farnesina, Rome, a masterpiece of the Italian Renaissance, with loggias frescoed by renowned artists such as Raffaello Sanzio. Plant leaves were sampled in September and December 2020 and lichen transplants were exposed from October 2020 to early January 2021 at increasing distances from the main trafficked road, Lungotevere Farnesina, introducing an outdoor vs. indoor mixed sampling design aimed at assessing the impact of vehicular particulate matter (PM) on the Villa Loggias. The magnetic properties of leaves and lichens - inferred from magnetic susceptibility values, hysteresis loops and first order reversal curves - showed that the bioaccumulation of magnetite-like particles, associated with trace metals such as Cu, Ba and Sb, decreased exponentially with the distance from the road, and was mainly linked to metallic emission from vehicle brake abrasion. For the frescoed Halls, ca. 30 m from the road, the exposure to traffic-related emissions was very limited or negligible. Tree and shrub leaves of the Lungotevere and of the Villa's Gardens intercepted much traffic-derived PM, thus being able to protect the indoor cultural heritage and providing an essential conservation service. It is concluded that the joint use of magnetic and chemical analyses can profitably be used for evaluating the impact of particulate pollution on cultural heritage within complex metropolitan contexts as a preventive conservation measure.

## 1. Introduction

Cultural heritage is heavily threatened by air pollution, not only historical buildings and manufacts exposed outdoors, but also those exposed in closed environments (de la Fuente et al., 2013; Grau-Bové and Strlič, 2013). Gases, and especially particulate matter (PM), act on the surfaces, creating dark layers ("soiling"), abrasion of materials, depletion and discoloration, that often result in irreversible damage to the operas, with a consequent artistic loss (Comite et al., 2019; Grossi and Brimblecombe, 2004). Therefore, the protection of cultural heritage from air pollution is of primary importance. Nevertheless, threshold values for air pollutants similar to those for the protection of human health are actually missing. In order to preserve the cultural heritage as much as possible, the International

* Corresponding author.
*E-mail address:* aldo.winkler@ingv.it (A. Winkler).

http://dx.doi.org/10.1016/j.scitotenv.2022.153729

Centre for the Study of the Preservation and Restoration of Cultural Property (ICCROM) promotes the approach of "preventive conservation", defined as: "all measures and actions aimed at avoiding and minimizing future deterioration or loss. These are carried out within the context or on the surroundings of an item, but more often a group of items, whatever their age and condition. These measures and actions are indirect – they do not interfere with the materials and structures of the items. They do not modify their appearance". Through the preventive conservation, the entire collection or the group of manufacts is protected as a whole, and it is economically more advantageous than the restoration of the single manufact (Lambert, 2010). In this view, the continuous monitoring of air quality assumes a central role at indoor exhibitions, since they are mostly located in urban areas where air pollution can penetrate inside through the normal air circulation and heating, ventilation and air conditioning (HVAC) systems, if suitable filters are not used (Hackney, 1984), and visitors and routine cleaning operations constantly introduce and re-suspend particles that remain for hours in the room air (Uring et al., 2020; Qian et al., 2008).

Lichen biomonitoring is a well-established technique for the assessment of air quality (Conti and Cecchetti, 2001): lichens are both very sensitive to phytotoxic air pollutants and able to accumulate trace elements well in excess of their nutritional requirements (Bačkor and Loppi, 2009) proportionally to atmospheric bulk (wet and dry) deposition (Loppi and Paoli, 2015). These techniques have been used mostly outdoors (e.g. Loppi, 2014; Contardo et al., 2020), but also indoors (Paoli et al., 2019a) including car cabins (Paoli et al., 2019b), and are used in epidemiological studies (Cislaghi and Nimis, 1997), environmental justice assessment (Contardo et al., 2018) and environmental forensics (Loppi, 2019). Being independent from their supporting substrate, lichens can be easily taken from a remote site and exposed in a study area following any suitable sampling design: in this way, both the initial concentrations of unexposed samples and the exposure time are known.

Trace elements bioaccumulated by lichens are often associated with the magnetic fraction of PM, i.e., magnetite-like ferrimagnetic particles (e.g. Flanders, 1994; Georgeaud et al., 1997; Hunt et al., 1984), mainly deriving from emission sources like brake abrasion, or iron oxides produced during combustion processes (Winkler et al., 2020; Gonet et al., 2021a, 2021b). Thus, the magnetic properties of bioaccumulated elements are an economically feasible and fast proxy for the anthropogenic fraction of PM, allowing to detect its main sources (for a review see Hofman et al., 2017).

In this work, we tested for the first time the use of lichen biomonitoring techniques for the preventive conservation of a historical building and its interiors: Villa Farnesina (Rome, Italy), with the aim of evaluating i) the air pollution dynamics from outside to inside of the building, ii) the influence of vehicle traffic, and iii) the magnitude of the deposition inside the building.

Lichen exposure was preceded by a feasibility study carried out on the magnetic properties of plant leaves sampled outside the Villa and inside its gardens. A second leaf sampling was carried out before retrieving the lichen transplant, to monitor the variation in the bioaccumulation of magnetic PM after three months of exposure to restored traffic conditions after the end of the strictest pandemic lockdown period, followed by summer holidays. In this sense, this work also explores the possibility to combine the use of lichen and plant leaves for biomonitoring PM in mixed outdoor and indoor contexts which are relevant for their cultural value.

The role of trees and shrubs is also explored for its important role in removing air pollutants, especially particulate ones, with dry deposition being the main pathway, especially in areas with scarce atmospheric precipitation such as the Mediterranean region (e. g, Blanusa et al., 2015). Urban and periurban forests, which are integrated within the concept of "green infrastructures", provide important ecosystem services, including air purification (Manes et al., 2016), and limit the adverse impact of particulate matter on cultural heritage within urban contexts.

It should be noted that this work was carried out under partial Covid19 restrictions, including the curfew imposed from October 26th at 10 PM, that heavily impacted on the traffic of the touristic and nightlife downtown of Rome. Above all, museums were closed to visitors for most of the period of lichens exposure. Further restrictions were imposed during Christmas holidays, in particular starting from December 21, 2020 until January 6, 2021. Thus, this study contributes to the evaluation of air pollution dynamics under limited polluting emissions and without the prolonged interference of visitors, that are, as mentioned above, important actors for the introduction and resuspension of particles.

As a summary, in this study it was tested if the Halls of Villa Farnesina are preserved from large inputs of vehicular magnetic particles – mainly brakes' emission – because of the distance from the main road and the ecosystem services provided by trees and shrubs, as assessed by means of multidisciplinary biomonitoring techniques.

## 2. Materials and methods

### 2.1. Study area

Villa Farnesina was built in the XVI century by the Italian architect Baldassarre Peruzzi for the Sienese banker Agostino Chigi, who appointed renowned artists such as Raffaello Sanzio, Sebastiano del Piombo, Giovanni Antonio Bazzi (called "Il Sodoma") for the internal decorations. For the volumetric harmony of the building, the artistic value of its frescoes and the beauty of the gardens, Villa Farnesina is regarded as one of the masterpieces of the Italian Renaissance. Today, the Villa is the headquarter of the worldwide renowned Accademia Nazionale dei Lincei, one of the oldest academic institutions promoting literature, arts, sciences and culture, whose current vice-President was recently awarded the Nobel Prize for Physics.

On the ground floor of the building, the Galatea as well as the Amore e Psiche Halls host impressive frescoes by Raffaello Sanzio; on the first floor, the Perspectives and Alessandro e Rossane's wedding Halls were painted by Baldassarre Peruzzi and Giovanni Antonio Bazzi, respectively. The back of the Villa (on the South side, at the present-day entrance) opens onto the "secret garden", designed after the 15th-century model of the *hortus conclusus* and is separated from the main gardens by a tall hedge. In the main gardens, cypress trees, pines and other ornamental tree and shrub species (i.e., roses, quinces, medlars, huisache, Acacia of Constantinople, ornamental citrus trees, cherry trees, oaks, ancient camellias, myrtles, oleanders) form a varied and colorful array along the ancient Farnese wall. The gardens extend parallel to the right bank of the Tiber River, separated by a perimeter brick and iron fence from the heavy trafficked one-way road Lungotevere Farnesina, which also serves as a congested vehicular parking on both sides (Fig. 1).

### 2.2. Leaf sampling

The first sampling was conducted on September 3, 2020 and involved leaves collected from various rows of trees and shrubs aligned at increasing distances from the roadside, selecting the species with at least three close trees available. In detail, the leaves of 11 *Platanus* sp. trees on the sidewalk of the Lungotevere road and, inside the gardens of the Villa, 7 *Cupressus sempervirens* - clone 'Bolgheri' trees close to the *Platanus*, 3 *Nerium oleander* shrubs in-between cypress and the building on the side of the Galatea Hall and 4 *Myrtus communis* trees in front of a window of the Galatea Hall were sampled at about 2–3 m from ground (Fig. 1a). Leaves were randomly taken mostly on the side facing the road, with the exception of *Platanus* 6S, that was sampled from a branch close to a cypress inside the Villa, Myrtle 2 whose leaves were sampled in both directions with respect to the road and Oleanders 2 and 3, that were sampled on the Villa side and on its top, respectively.

The *Platanus sp,* trees are distant about 7 m each other, almost regularly spaced all along Lungotevere Farnesina, with their crowns in close contact during the growing season. Cypresses are distant 4 m each other, and their evergreen crowns are not in contact. Oleanders are distant about 2 m each other, and myrtles, with their evergreen crowns in close contact, 4 m spaced.

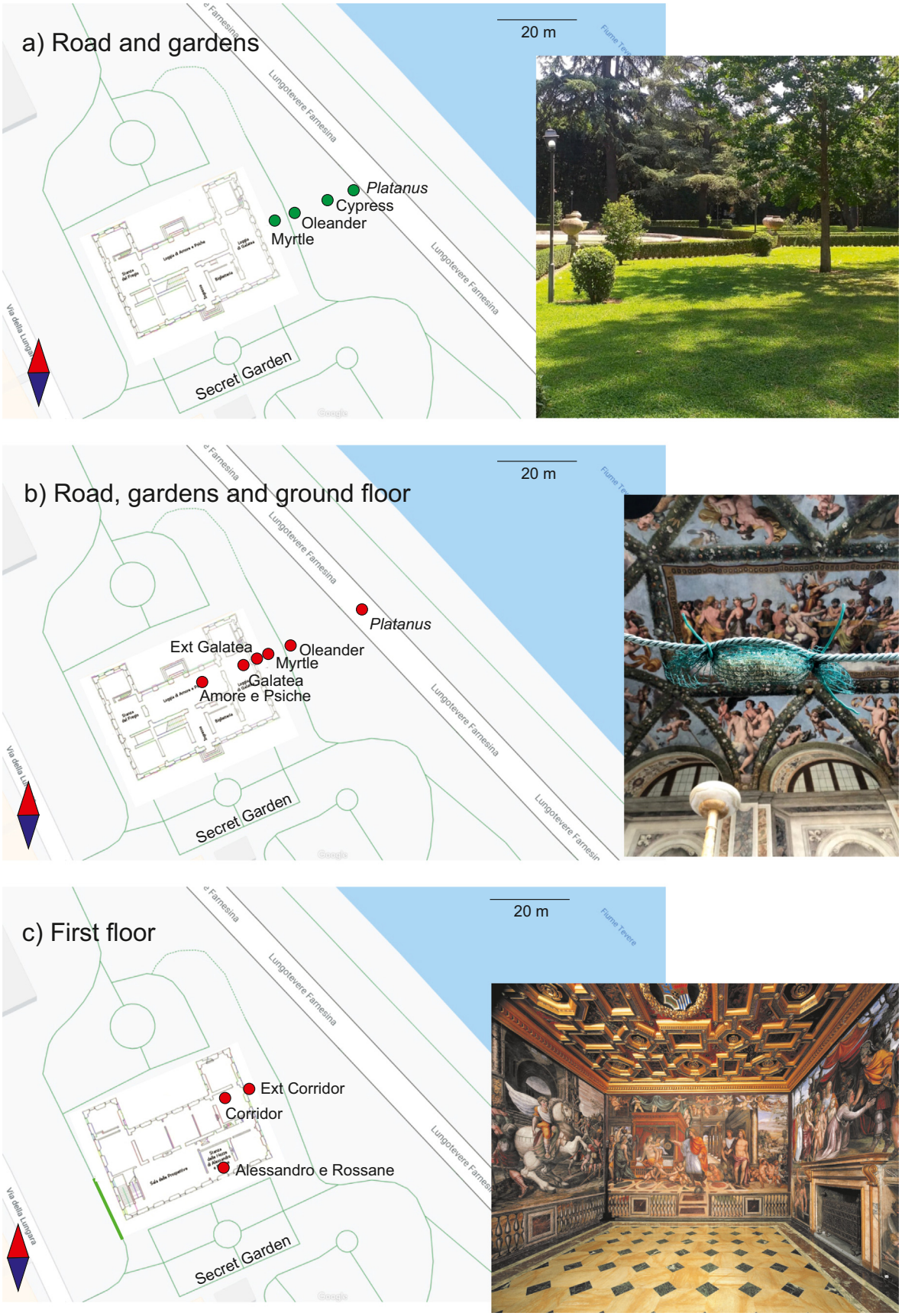


**Fig. 1.** Map of Villa Farnesina, reporting leaf (a) and lichen (b, c) samplings: each point represents a row of trees (green) or a group of three lichen bags (red) sampled or exposed at similar distances from the road. The light green lines indicate pedestrian paths inside the gardens and along the Tiber bank. In the insets, the gardens (a), Amore e Psiche (b) and Alessandro e Rossane's (c) Halls are shown. A perimeter brick and iron fence separates the cypresses of the Villa from the sidewalk were *Platanus* trees are.

On the second sampling, carried out on December 18, 2020, it was possible to collect the not yet fallen leaves of 7 *Platanus* trees, together with 6 cypresses, 3 oleanders and 4 myrtles, with the same sampling design adopted in September; in this occasion, to increase the dataset, *Platanus* leaves were sampled also on the sidewalk of the Tiber river, without any difference from the traffic point of view, since Lungotevere Farnesina is one-way.

### 2.3. Lichen material and sampling design

The lichen *Evernia prunastri* (L.) Ach. was selected as suitable biomonitor for this study, being a species widely used in biomonitoring surveys (Loppi et al., 2019). The lichen material was collected in a pristine area of Central Italy (Siena, Tuscany), selecting healthy thalli of similar size thus similar age, to reduce the natural variability due to age and size (Wolterbeek and Bode, 1995), from tree branches at least 1.5 m above ground to avoid possible soil contamination of samples. In the laboratory, samples were quickly washed with deionized water, and extraneous particles such as moss and bark fragments were removed using plastic tweezers. Lichen samples were organized in lichen bags of homogeneous size, using a plastic net loosely bound and closed at the extremities. The exposure of the samples lasted three months (from October, 12, 2020 to January, 8, 2021), which is optimal for this species (Loppi et al., 2019). The exposure was terminated immediately before the beginning of restoration works of the Galatea Hall, to avoid sample contamination. Once exposed, samples were sprayed with deionized water once per week to allow a sufficient humidity for the thallus metabolism. After the exposure, samples were retrieved, air dried and stored at −20 °C until magnetic and chemical analysis.

Following the exposure of the Villa to a busy road, a linear transect was drawn from Lungotevere Farnesina to the inside of the building, selecting six sites outside and at the ground floor (Fig. 1b), and three sites at the first floor of the Villa (Fig. 1c), including two corresponding windows that were left open for most of the duration of the experiment in order to favor ventilation for preventing the pandemics, and sporadically closed during rainfall events.

Lichens were exposed on *Platanus* trees at both roadsides of Lungotevere Farnesina and, at the ground level of the Villa complex, at increasing distance from the road and towards the Halls, on an oleander and a myrtle in close contact and aligned parallel to the road, on a myrtle in front of the window of Galatea Hall, on the external window frame of Galatea Hall, inside Galatea Hall, inside Amore e Psiche Hall. On the first floor of the Villa, the bags were exposed on the external window frame of a corridor, inside a corridor, and inside the Alessandro e Rossane's wedding Hall. The ground floor and the gardens of Villa Farnesina are below the road level, which is roughly located at half height between its ground and the first floor. Indoor lichen bags were tied to non-metallic furniture. Outside the building, the samples were tied to tree branches at least 2 m from ground while, inside the Villa, the samples were tied to the velvet ropes behind the frescoed walls at ca 50 cm from ground (it was the only possibility). Two sets of samples were located just below the external window frames (one for each floor) to catch the bioaccumulation of trace elements as close as possible to the Villa interiors. At each site, three lichen bags (replicates) were exposed. Six samples were left unexposed and kept at −20 °C until analysis. Two different batches of three unexposed samples were used in this study: samples brought to the sampling site and stored without being exposed to check any possible influence of the travel to the exposure site (unexposed), and samples stored in the laboratory immediately after harvest (pre-transplant).

### 2.4. Chemical analysis

Lichen samples were powdered and homogenized and about 200 mg of each sample were acid-digested using a mixture of 3 mL 70% of $HNO_3$, 0.2 mL of HF, and 0.5 mL of $H_2O_2$ in a microwave digestion system (Ethos 900, Milestone). The content of Al, Ba, Cd, Cr, Cu, Fe, Ni, Sb, Sn, Zn was then quantified by ICP-MS (Sciex Elan 6100, PerkinElmer). A procedural blank and a sample of the certified materials IAEA 336 "Lichen" were included in each set of analysis. Recoveries were in the range 91% (Al) – 112% (Zn); precision of the analysis, estimated by the coefficient of variation of five replicates, was within 10% for all elements. The results are expressed on a dry weight basis.

### 2.5. Magnetic analysis

Leaf and lichen samples were dried at 40 °C with a Bionsec Domus plastic desiccator, to avoid any metal contamination, and then placed into standard 8 $cm^3$ palaeomagnetic plastic cubes for magnetic susceptibility analyses or fragmented inside pharmaceutical gel caps #4 for the hysteresis and FORC (first order reversal curves) characterizations.

Mass magnetic susceptibility ($\chi$) was calculated dividing the values measured with a Agico KLY5 meter for the net weight of the samples. The coercive force ($B_c$), the saturation remanent magnetization by mass ($M_{rs}$, or SIRM) and the saturation magnetization by mass ($M_s$) were determined with a vibrating sample magnetometer (VSM Micromag 3900, Princeton Magnetics) at a maximum field of 1.0 T; concentration dependent hysteresis parameters were calculated subtracting the high field paramagnetic linear trend before dividing the magnetic moments for the net weight of the samples. The coercivity of remanence ($B_{cr}$) values were interpolated from backfield remagnetization curves up to −1 T, after saturating at 1 T field.

The domain state and magnetic grain-size of the samples were compared to theoretical magnetite according to the hysteresis ratios $M_{rs}$ / $M_s$ vs. $B_{cr}$ / $B_c$ in the "Day plot" (Day et al., 1977; Dunlop, 2002a, 2002b).

FORCs were measured in steps of 2.5 mT, with 300 ms averaging time and maximum applied field being 1.0 T using a Lakeshore 8604 VSM; FORC diagrams were processed, Variforc smoothed and drawn with the FORCINEL 3.05 Igor Pro routine (Harrison and Feinberg, 2008): relatively high smoothing factors on the vertical and horizontal ridges (4 to 6), even larger on the backgrounds, were selected due to the weak magnetic properties of the samples. FORC diagrams provide information regarding magnetic reversal mechanisms in ferromagnetic minerals (Pike et al., 1999; Roberts et al., 2000): they are used for delineating the distributions of the interaction field ($B_u$) and coercivity in samples and to distinguish between single domain (SD), multidomain (MD) and pseudo-single domain (PSD) behaviors, the latter recently referred as "vortex state" for better describing the transitional state between SD and MD.

### 2.6. Deposition rate

The element concentration found in lichens can effectively be used to estimate a deposition rate (Loppi, 2014; Loppi and Pirintsos, 2003; Loppi, 2019; Contardo et al., 2020). After cutting small pieces of thallus lobes, we measured the dry weight and the area of these fragments, obtaining a mean weight/area ratio of 160 μg/$m^2$. The deposition rate was then calculated considering the final concentration as an equilibrium value with the environment reached in 3 months of exposure according to the formula:

$$\text{deposition}\ \left(\mu g\ m^{-2}\ d^{-1}\right) = \text{concentration}\ \left(\mu g\ g^{-1}\right) \times 160\ \left(g\ m^{-2}\right)/90\ (\text{days})$$

### 2.7. Statistical analysis

Descriptive statistics were calculated using Microsoft Excel and Past 4.05 software (Hammer et al., 2001). The correlation analysis between magnetic and chemical data was run using the Pearson coefficient of linearity.

## 3. Results

### 3.1. Magnetic properties of leaves

The magnetic susceptibility of plant leaves sampled in September (Table 1s) ranged between −0.02 and 22.31 × $10^{-8}$ $m^3$ $kg^{-1}$, with mean values ± standard error, averaged by tree species, 7.86 ± 1.01, 15.20 ±

2.36, 2.07 ± 1.20 and 0.96 ± 0.53 × $10^{-8}$ $m^3$ $kg^{-1}$ for *Platanus*, cypress, oleander and myrtle (from closest to farthest from road), respectively.

The hysteresis loops were saturated well before 1 T, with modest coercivities: 4.8 mT < $B_c$ < 8.2 mT and 29.6 mT < $B_{cr}$ < 40.6 mT.

Concentration dependent hysteresis parameters $M_s$ and $M_{rs}$ ranged between 1.7 and 21.1 $mAm^2kg^{-1}$ and 0.1 and 1.6 $mAm^2kg^{-1}$, respectively, and varied in the same way as the magnetic susceptibility, with respect to the distance from the roadside, with mean values of $M_s$ = 7.9 ± 0.9, 13.9 ± 2.1, 2.4 ± 0.7, 2.1 ± 0.4 $mAm^2kg^{-1}$ and mean values of $M_{rs}$ = 0.6 ± 0.1, 1.0 ± 0.2, 0.1 ± 0.0, 0.2 ± 0.0 $mAm^2kg^{-1}$, for *Platanus*, cypress, oleander and myrtle, respectively.

The samples Oleander 1S, 2S and 3S were sampled facing the road, the Villa and over its top, respectively, and the magnetic susceptibility values seem to follow this directional variability (Fig. 2a), that was not further explored in this study, to maintain a site averaged statistic approach. Overall, the concentration-dependent magnetic parameters indicated concentrations of ferrimagnetic minerals decreasing in the sequence χ, $M_s$, $M_{rs}$ (cypress) > χ, $M_s$, $M_{rs}$ (*Platanus*) > χ, $M_s$, $M_{rs}$ (oleander) > χ, $M_s$, $M_{rs}$ (myrtle); see Fig. 2a for χ.

In the "Day plot" (Fig. 3), the data points, calculated as mean $B_{cr}/B_c$ and $M_{rs}/M_s$ ratios for each species, fell in the middle-right side of the plot, between the theoretical curves calculated for mixtures of SD and MD magnetite grains and that for a mixture of SD and superparamagnetic (SP) magnetite grains.

The FORC diagrams of *Platanus* (Fig. 4a) and cypress (Fig. 4c) leaves, selected for their relatively intense magnetic properties, were very similar, with their distribution peaking close to the origin of the diagram and dominated by typical MD grain features, such as the vertical distribution along the Bu axis (Roberts et al., 2000), with a sharp tail extending to higher coercivities.

In December, the deciduous *Platanus* leaves, at the end of their life cycle, showed a distinctively higher magnetic susceptibility value (Table 2s), with a mean χ (18.4 ± 4.6 × $10^{-8}$ $m^3$ $kg^{-1}$) higher than in September; conversely, the evergreen cypress leaves showed a lower magnetic susceptibility (χ = 9.4 ± 1.3 × $10^{-8}$ $m^3$ $kg^{-1}$), than in September. At increasing distance from the road, mean values for oleanders and myrtles were χ =

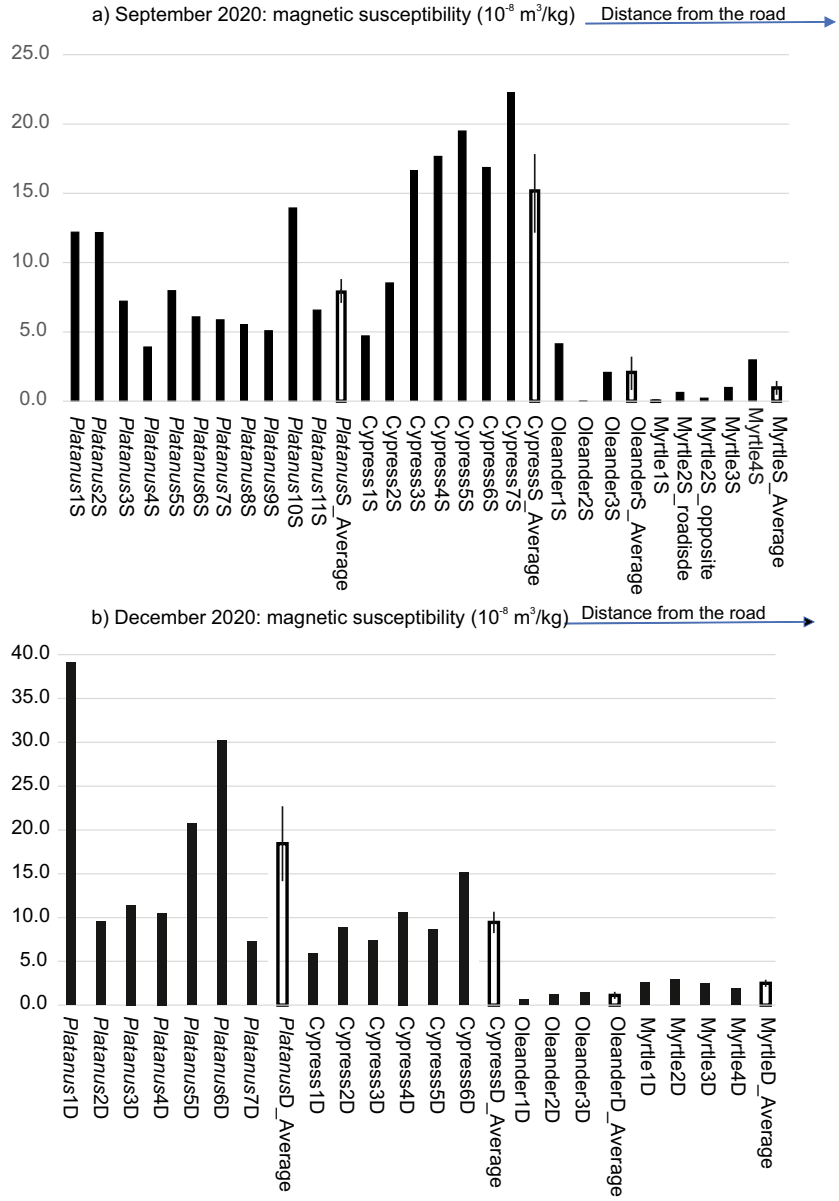


**Fig. 2.** Histograms of mass magnetic susceptibility of plant leaves, sampled in (a) September, suffix "S" and (b) December, suffix "D": black bars = individual trees, white bars = site averages, with standard errors. The species are ordered from left to right, at increasing distances from the road. Myrtle 2 was sampled in September on both directions with respect to the road.

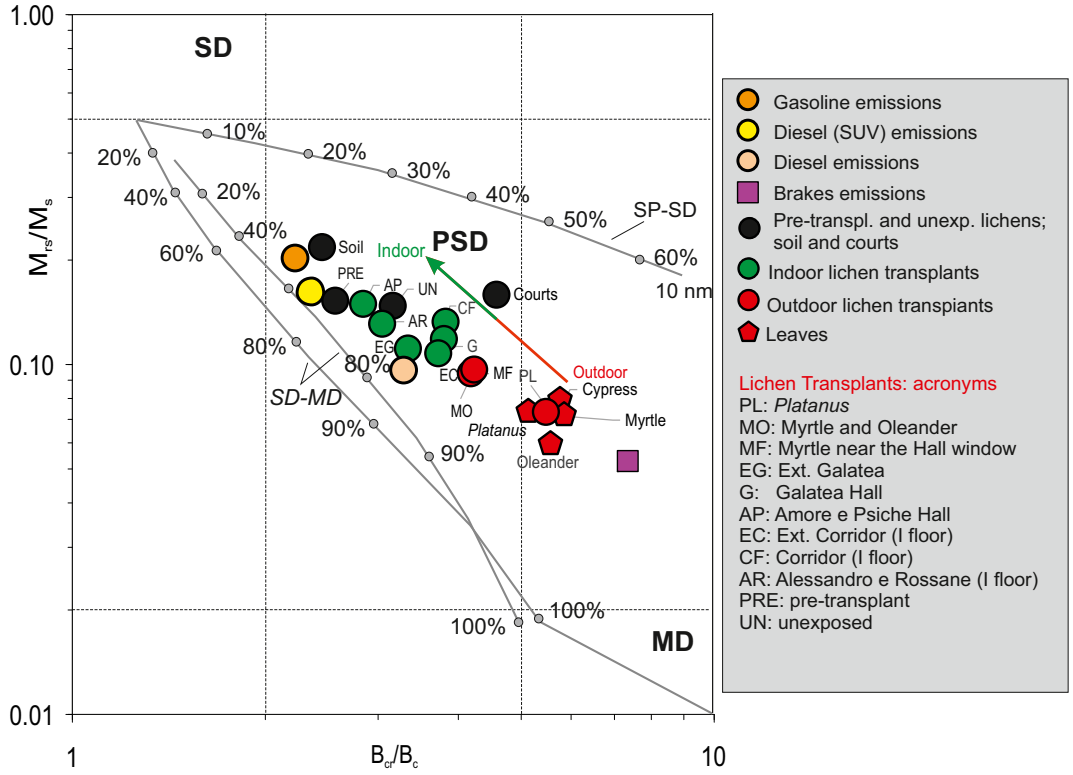


**Fig. 3.** Bilogarithmic "Day plot" (Day et al., 1977) of the site averaged hysteresis ratios for leaves and lichen transplants (pentagons and circles, respectively; red symbols outdoor samples, green circles indoor lichens), reported together with the average points for different kinds of fuel exhaust (orange, yellow and pink circles) and brake dust particles (purple square) calculated from Sagnotti et al., 2009. The SD (single domain), PSD (pseudo-single domain) and MD (multidomain) fields and the theoretical mixing trends for SD-MD and SP-SD pure magnetite particles (SP, superparamagnetic) are from Dunlop (2002a, 2002b). Unexposed, pre-transplant, soil of the gardens and court samples are reported as black circles. The outdoor samples are located at the middle-right side of the plot, near the brakes data, while the indoor transplants fall in the central part of the plot, close to the unexposed and pre-transplant control samples.

$1.1 \pm 0.2$ and $2.5 \pm 0.2 \times 10^{-8}$ $m^3$ $kg^{-1}$, thus, respectively lower and higher than those reported in September (Fig. 2b).

### 3.2. Magnetic properties of lichens

The magnetic susceptibility of lichens (Table 1), at site level, was computed as the mean of three replicates, and varied as $\chi = 24.5 \pm 5.4$, $6.6 \pm 1.2$, $3.8 \pm 0.3$, $2.4 \pm 0.3$, $1.0 \pm 0.0$, $1.0 \pm 0.2 \times 10^{-8}$ $m^3$ $kg^{-1}$ for bags exposed outside the Villa on *Platanus* trees and, on the Villa's ground level, tied to a oleander and a myrtle closely aligned at the same distance from the roadside, to a myrtle in front of the window of Galatea Hall, to the external window frame of Galatea Hall, inside Galatea Hall, inside Amore e Psiche Hall, listed at increasing distance from the road. On the first floor, $\chi = 1.8 \pm 0.1$, $0.7 \pm 0.2$, $0.7 \pm 0.2 \times 10^{-8}$ $m^3$ $kg^{-1}$ for bags exposed on the external windows frame of a corridor, inside a corridor, and inside Alessandro e Rossane's wedding Hall. Based on mean $\chi = 0.6 \pm 0.3 \times 10^{-8}$ $m^3$ $kg^{-1}$ for the three unexposed samples, a ratio of the magnetic susceptibility of exposed to unexposed samples was calculated, resulting 39.3, 10.6, 6.1, 3.9, 1.6, 1.5 for the ground floor and 2.9, 1.2 and 1.1 for the first floor, adopting the same sequence as before.

The hysteresis loops were saturated well below 1 T, with mean coercivities $6.6\ mT < B_c < 13.3\ mT$ and $33.3\ mT < B_{cr} < 49.4\ mT$, which are slightly higher than those determined for leaves.

Concentration dependent hysteresis parameters $M_s$ and $M_{rs}$ varied consistently with the magnetic susceptibility with respect to the distance from the roadside and the floor, i.e., $M_s$ decreasing from $18.9 \pm 2.5$ to $1.4 \pm 0.3$ $mAm^2/kg$ and $M_{rs}$ from $1.4 \pm 0.2$ to $0.2 \pm 0.0$ $mAm^2/kg$, adopting the same order of magnetic susceptibility data.

In the Day plot (Fig. 3), as the distance from the roadside increases, the lichen points tend to migrate from the middle-right side of the plot, where leaf points are located, towards the central part of the plot, thus approaching the trend lines for theoretical mixtures of SD-MD pure magnetite and the points of the control samples.

Lichens exposed near the road and those exposed indoors form two well separated clusters, with samples exposed just outside the building at mid-distances from the road, falling in between.

The control samples resulted not "magnetically pristine", in the sense that they are not purely diamagnetic or paramagnetic: in the "Day plot", their average points fell in same upper-central region of the samples exposed inside the Halls.

The FORC diagrams reflect the same trend of the "Day plot": MD features prevail for the lichens exposed on *Platanus* (Fig. 4b), with a magnetic component peaked at $B_c \sim 20$ mT emerging at increasing distance from the road, until becoming the prevalent coercivity component in the lichens exposed in the Amore e Psiche Hall (Fig. 4e) and in a pre-transplant sample (Fig. 4f).

Overall, the concentration of soft ferrimagnetic minerals, as deduced from concentration dependent magnetic parameters, are strongly dependent on distance from the road, as shown with the barplot of magnetic susceptibility and the magnetic susceptibility ratio with respect to the distance from the road (Fig. 5a, b); in (b), the distances were approximately evaluated through the Google Earth web application, and verified though a laser telemeter, and are referred to the sidewalk closest to the Tiber River, the farther with respect to the Villa.

### 3.3. Bioaccumulation of trace elements

The relationship of trace elements accumulated in lichen transplants with distance from the road followed the same trend as their concentration dependent magnetic properties (Table 3s) The highest concentrations were recorded on *Platanus*, at the Lungotevere road,

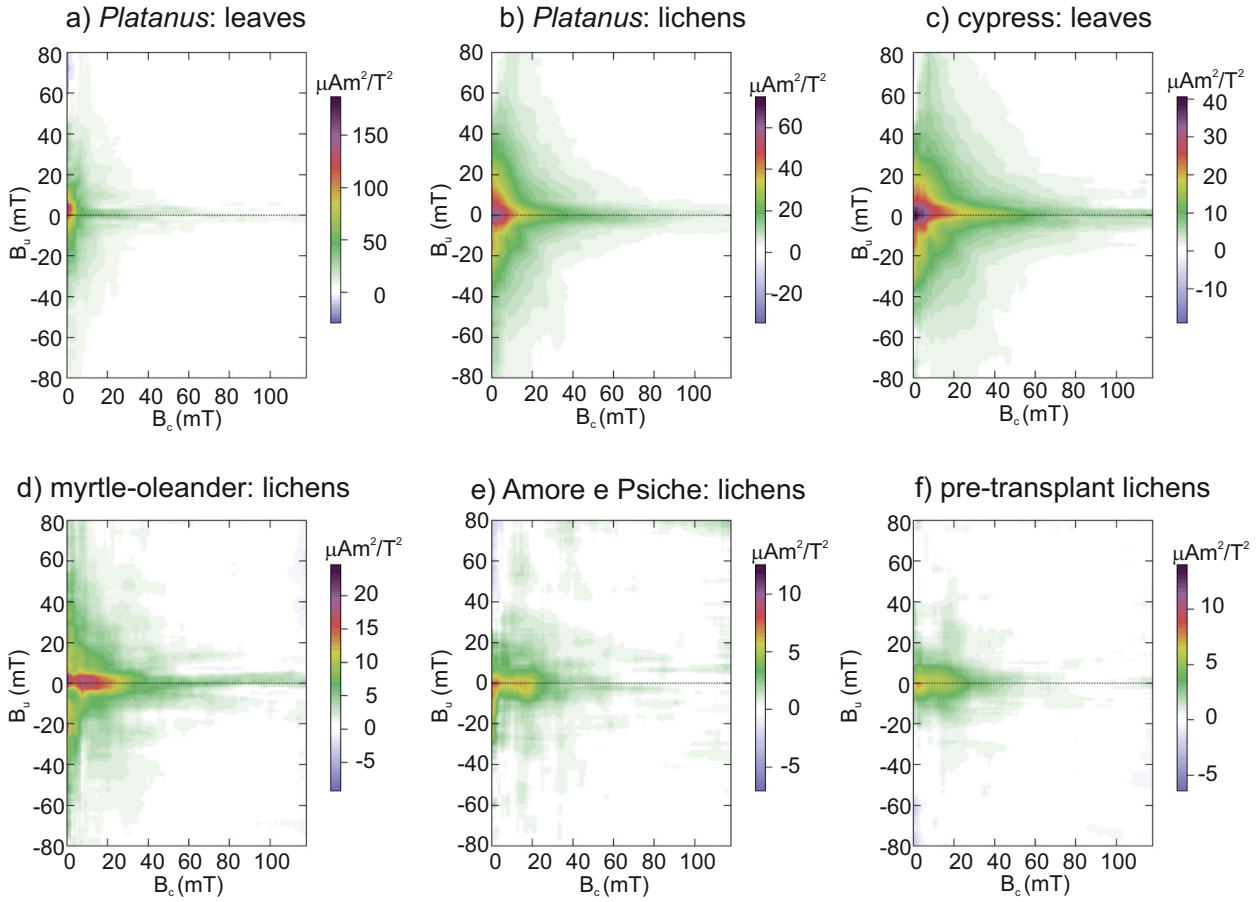


**Fig. 4.** FORC diagrams, for September leaves (a, c) and lichens (b, d, e, f): multidomain (MD) features prevail for the samples exposed outdoor and near the Lungotevere Farnesina busy road, while single domain (SD) characteristics emerge for the unexposed samples and for those exposed at higher distance from the road and inside the Amore e Psiche Hall. $B_u$ is the interaction field, $B_c$ the coercivity.

and the lowest inside the halls of Villa Farnesina, with some elements (Al, Ba, Cr, Cu, Fe, Sb) showing higher values in the Amore e Psiche hall, compared with the other rooms. Arranging the data according to road, garden, indoor ground floor, outdoor 1st floor, indoor 1st floor (Table 4s), a clear decreasing trend emerged with the distance from the road. The data also highlight that the Halls, at the ground floor, experience overall slightly higher elemental levels compared with the 1st floor, regardless of outdoors or indoors, which in turn showed values very similar to those of unexposed samples.

The average annual element deposition rates at the exposure sites were also estimated based on lichen bioaccumulation data (Table 4s).

### 3.4. Correlation between $\chi$, $M_s$ and $M_{rs}$ vs. element concentration

The linear correlation between the concentration dependent magnetic parameters ($\chi$, $M_s$ and $M_{rs}$) and the concentration of Al, Ba, Cd, Cr, Cu, Fe, Ni, Sn, Sb and Zn was tested, at site level, for lichens (Table 5s; Fig. 6). $\chi$, $M_s$ and $M_{rs}$ were linearly correlated ($p < 0.05$) for all the elements but Al ($p > 0.17$ for $\chi$, $M_s$ and $M_{rs}$) and Cr, that was at the significance threshold for $\chi$ and $M_s$, and significant for $M_{rs}$. Interestingly, Al, an element of limited metabolic value in lichens and commonly used as tracer of geogenic input, was not at all correlated with magnetic parameters.

## 4. Discussion

### 4.1. Magnetic susceptibility of leaves and lichens

In both lichens and leaves, the magnetic parameters $\chi$, $M_s$ and $M_{rs}$ were strongly correlated, suggesting that they are indicative of the same magnetic fraction, with the magnetic susceptibility well representing the concentration of ferromagnetic particles in PM. Moreover, the significant correlations demonstrate that the gel caps, despite their small volume, are suitable for representing the overall ferromagnetic fraction of lichens and leaves, and that PM is homogenously bioaccumulated.

The magnetic susceptibility values of plant leaves, considering both the September and December collections, ranged from $-0.02$ to $39.10 \times 10^{-8}$ $m^3\,kg^{-1}$, highlighting a large variability spanning over two orders of magnitude, which was strongly related to the distance from the roadside (Fig. 2 a, b). The highest values of $\chi$ were measured for *Platanus* leaves, which showed an average increase from 7.86 to $18.42 \times 10^{-8}$ $m^3kg^{-1}$ from September to December, indicating a relevant bioaccumulation of magnetic particles after the end of the strictest lockdown measures for containing the Covid-19 pandemic. This outcome is consistent with the doubling of magnetic susceptibility values of $PM_{10}$ filters exposed in trafficked urban contexts after the end of the strictest lockdown phase, when vehicular traffic promptly increased (Winkler et al., 2021). The aforementioned study was based on the filters sampled at Magnagrecia urban traffic station, at about 2 km from Villa Farnesina, where average $PM_{10}$ concentration was 27 μg $m^{-3}$ for the year 2020, similarly to Largo Argentina station, 1 km far from the Villa, where the average $PM_{10}$ concentration during the lichen exposure was 25.8 μg $m^{-3}$.

In September, the magnetic susceptibility of 5-months-old *Platanus* leaves was lower than that of cypress leaves; conversely, in December *Platanus* leaves showed higher magnetic susceptibility values compared to cypress, whose magnetic susceptibility decreased. Moreno et al. (2003) suggested that the evergreen or deciduous nature of leaves, as observed on *Platanus sp* and *Quercus Ilex* leaves, drives the magnetic susceptibility values, which are primarily influenced by the distance from the road;

**Table 1**
Average, standard deviation (sd), minimum and maximum values of mass specific magnetic susceptibility ($\chi$), saturation magnetization ($M_s$), remanent magnetization ($M_{rs}$), coercivity ($B_c$), coercivity of the remanence ($B_{cr}$) and saturation remanent magnetization to magnetic susceptibility ratio (SIRM/$\chi$) of the lichen bags, unexposed and pre-transplant control samples.

| | | $\chi$ ($10^{-8}$ $m^3$ $kg^{-1}$) | $M_s$ ($mAm^2/kg$) | $M_{rs}$ ($mAm^2/kg$) | $B_c$ (mT) | $B_{cr}$ (mT) | SIRM/$\chi$ (kA/m) |
|---|---|---|---|---|---|---|---|
| *Platanus* | mean | 24.5 | 18.9 | 1.4 | 6.6 | 36.1 | 6.2 |
| | sd | 9.3 | 4.5 | 0.3 | 0.4 | 2.0 | 2.7 |
| | min | 13.8 | 15.7 | 1.1 | 6.2 | 33.4 | 3.7 |
| | max | 30.7 | 24.0 | 1.7 | 7.1 | 38.0 | 9.1 |
| Myrtle - Oleander | mean | 6.6 | 7.0 | 0.7 | 8.7 | 36.3 | 11.1 |
| | sd | 2.1 | 2.1 | 0.2 | 0.2 | 0.3 | 6.1 |
| | min | 4.2 | 4.7 | 0.4 | 8.5 | 36.0 | 5.1 |
| | max | 8.3 | 8.7 | 0.8 | 8.9 | 36.6 | 17.2 |
| Myrtle | mean | 3.8 | 3.8 | 0.3 | 9.5 | 39.8 | 8.9 |
| | sd | 0.6 | 1.5 | 0.1 | 1.2 | 1.7 | 1.5 |
| | min | 3.2 | 2.2 | 0.2 | 8.6 | 37.9 | 7.2 |
| | max | 4.4 | 5.0 | 0.4 | 10.9 | 41.2 | 9.8 |
| Ext Galatea | mean | 2.4 | 2.5 | 0.3 | 9.9 | 33.3 | 11.2 |
| | sd | 0.5 | 0.5 | 0.1 | 0.7 | 1.2 | 2.0 |
| | min | 1.9 | 2.1 | 0.2 | 9.2 | 32.1 | 8.9 |
| | max | 3.0 | 3.0 | 0.4 | 10.4 | 34.5 | 12.8 |
| Galatea | mean | 1.0 | 1.0 | 0.1 | 11.5 | 42.7 | 11.0 |
| | sd | 0.1 | 0.4 | 0.1 | 1.1 | 7.9 | 4.5 |
| | min | 0.9 | 0.6 | 0.1 | 10.3 | 37.8 | 6.2 |
| | max | 1.1 | 1.4 | 0.2 | 12.5 | 51.9 | 15.1 |
| Amore e Psiche | mean | 1.0 | 1.2 | 0.2 | 13.3 | 38.2 | 20.5 |
| | sd | 0.3 | 0.3 | 0.1 | 0.8 | 1.9 | 8.7 |
| | min | 0.8 | 1.0 | 0.1 | 12.4 | 36.5 | 11.0 |
| | max | 1.3 | 1.6 | 0.2 | 13.8 | 40.3 | 28.0 |
| Ext Corridor | mean | 1.8 | 1.5 | 0.2 | 11.7 | 43.5 | 10.1 |
| | sd | 0.1 | 0.3 | 0.0 | 1.7 | 6.0 | 1.8 |
| | min | 1.7 | 1.3 | 0.2 | 10.1 | 40.0 | 8.7 |
| | max | 1.9 | 1.7 | 0.2 | 13.5 | 50.4 | 12.1 |
| Corridor | mean | 0.7 | 0.9 | 0.1 | 12.9 | 49.4 | 17.2 |
| | sd | 0.3 | 0.2 | 0.1 | 0.6 | 6.7 | 2.9 |
| | min | 0.4 | 0.7 | 0.1 | 12.3 | 45.2 | 14.2 |
| | max | 1.1 | 1.1 | 0.2 | 13.4 | 57.1 | 20.1 |
| Alessandro e Rossane | mean | 0.7 | 1.4 | 0.2 | 11.8 | 36.1 | 28.3 |
| | sd | 0.2 | 0.5 | 0.1 | 0.2 | 3.2 | 13.4 |
| | min | 0.5 | 0.9 | 0.1 | 11.5 | 32.5 | 18.7 |
| | max | 0.9 | 1.8 | 0.2 | 11.9 | 38.6 | 43.7 |
| Unexposed | mean | 0.6 | 0.9 | 0.1 | 13.0 | 41.6 | 29.1 |
| | sd | 0.6 | 0.4 | 0.1 | 0.3 | 3.1 | 16.0 |
| | min | 0.0 | 0.3 | 0.0 | 12.7 | 39.5 | 10.1 |
| | max | 1.2 | 1.2 | 0.2 | 13.2 | 45.1 | 49.2 |
| Pre-transplant | mean | 1.0 | 1.2 | 0.2 | 14.4 | 37.2 | 19.8 |
| | sd | 0.3 | 0.1 | 0.0 | 0.9 | 1.7 | 6.9 |
| | min | 0.6 | 1.1 | 0.2 | 13.5 | 35.2 | 12.7 |
| | max | 1.2 | 1.3 | 0.2 | 15.6 | 39.5 | 29.1 |

they also reported that the magnetic susceptibility of *Platanus* leaves ranged from 0.1 to 10.4 × $10^{-8}$ $m^3$ $kg^{-1}$ for wet leaves sampled in October, consistently with this study and lower with respect to the December 2020 leaves, whose values were in the same range of the more efficient *Quercus Ilex* leaves sampled in 2002. In general, these results suggest that it is inappropriate to compare the concentration-dependent magnetic parameters of leaves of different plant species, and that several factors influence their values, beyond the distance from the roadside and the deciduous or evergreen leaf traits. Plant species with a combination of leaf traits such as high trichome density and leaf wettability can have a higher accumulation of particles, thus being preferable as PM filters and for the mitigation of atmospheric PM: Muhammad et al. (2019) classified *Platanus x acerifolia* in the group characterized by the lowest SIRM values, while *Cupressaceae* fell in the medium and highest SIRM values classes. Thus, it is possible to suggest that the higher $\chi$ values of cypress leaves in September well represent their longer exposure to traffic and their bioaccumulation efficiency with respect to *Platanus*, whose $\chi$ values emerged in December, when the distance from the roadside – after prolonged exposure to vehicular traffic - was the main factor controlling the bioaccumulation of magnetic particles.

The magnetic susceptibility of cypress leaves decreased in December, with respect to September; it is supposed that $\chi$ decreased as a washing effect of the intense rainfalls occurring for 10 consecutive days before the sampling, even if Muhammad et al. (2020), through specific leaf washing experiments, reported a very limited washing effect in *Cupressaceae*. Blanusa et al. (2015) demonstrated that the leaf surface of *Platanus x hispanica*, owing to the presence of fine firm trichomes, was able to immobilize more than 90% of the total deposited particles, and Hofman et al. (2014), examining the leaf SIRM of *P. x acerifolia* for an entire growing season, observed a steady increase in leaf SIRM until the onset of senescence. Conversely, Muhammad et al. (2020) calculated that the immobilized fraction of PM raised from 36% to 54% from June to September in *Platanus* × *acerifolia*.

For oleanders and myrtles, the effect of distance from the roadside was dominant, with $\chi$ values, on average, respectively 13.6% and 6.3% of *Platanus* in September and respectively changing to 6.0% and 13.5% in December, not excluding that these variations can be linked also to larger errors arising from the experimental procedure affecting low magnetic susceptibility values: oleanders were considered efficient magnetic biomonitors by Moreno et al. (2003) second only to *Quercus Ilex*, as appreciated measuring and comparing different leaves of tree and shrubs species exposed side by side in Rome.

The magnetic susceptibility of lichen transplants clearly decreased with distance from the roadside, highlighting vehicular traffic as the main source of the bioaccumulated particles (Fig. 7); the exposed to unexposed magnetic susceptibility ratio decreased in the sequence 39.3, 10.6, 6.1, 3.9, 1.6, 1.5 for the ground floor and 2.9, 1.2, 1.1 for the first floor, following an exponential decay with distance from the roadside, as approximately estimated according to the Google Earth website application (Fig. 5b) and verified with a laser telemeter, and in agreement with Szönyi et al. (2008), who found that $\chi$ values decrease to a magnetic background level 20–30 m away from high-traffic roads.

Higher concentration dependent magnetic parameters are typically measured with increasing proximity to PM sources, and with increasing source strength (e.g., traffic volume): examples of such magnetic distance-decay are evident in magnetic biomonitoring studies for leaves (Matzka and Maher, 1999; Moreno et al., 2003; Hofman et al., 2016; Maher et al., 2008, Kardel et al., 2012; Hansard et al., 2012; McIntosh et al., 2007), lichens and mosses (Salo et al., 2016; Marié et al., 2016; Winkler et al., 2020).

The magnetic susceptibility of lichens transplanted inside the Halls was basically unaffected by the exposure, with a modest bioaccumulation of magnetic particles at the sensitivity limits of these measurements, and largely irrespective of Villa Farnesina floor.

Lichen transplants thus proved to be efficient and sensitive biomonitors, suitable for investigating the diffusion of PM particles inside unvegetated areas such as the Halls, without the uncertainty and variability connected to the use of leaves of different plant species.

The biomonitoring efficiency of lichens was further confirmed computing the difference of leaf magnetic susceptibility between December and September for *Platanus*, Oleander and Myrtle, and comparing the results with the magnetic susceptibility of lichens exposed on the same sites, after being corrected for the mean magnetic susceptibility of unexposed samples.

Under the same location and exposure period, lichens always showed higher increases of magnetic susceptibility than leaves: 23.9, 6.0, 3.2 × $10^{-8}$ $m^3$ $kg^{-1}$ vs 10.6, −1.0, 1.5 × $10^{-8}$ $m^3$ $kg^{-1}$, respectively for lichens and leaves exposed or sampled on *Platanus*, Oleander and Myrtle, respectively.

Distance from the roadside preserved the Halls from large inputs of vehicular magnetic particles, but a joint protective effect was offered by the trees and shrubs of the Lungotevere and the gardens that, according to the magnetic susceptibility values, played an important role in accumulating and removing particulate pollutants from the air, thus providing an important ecosystem service to Cultural Heritage.

Green spaces can improve air quality through dry deposition on the leaf surface (Blanusa et al., 2015), working as a natural sink for pollutants, as suggested by several authors (Fusaro et al., 2017; Mukherjee and

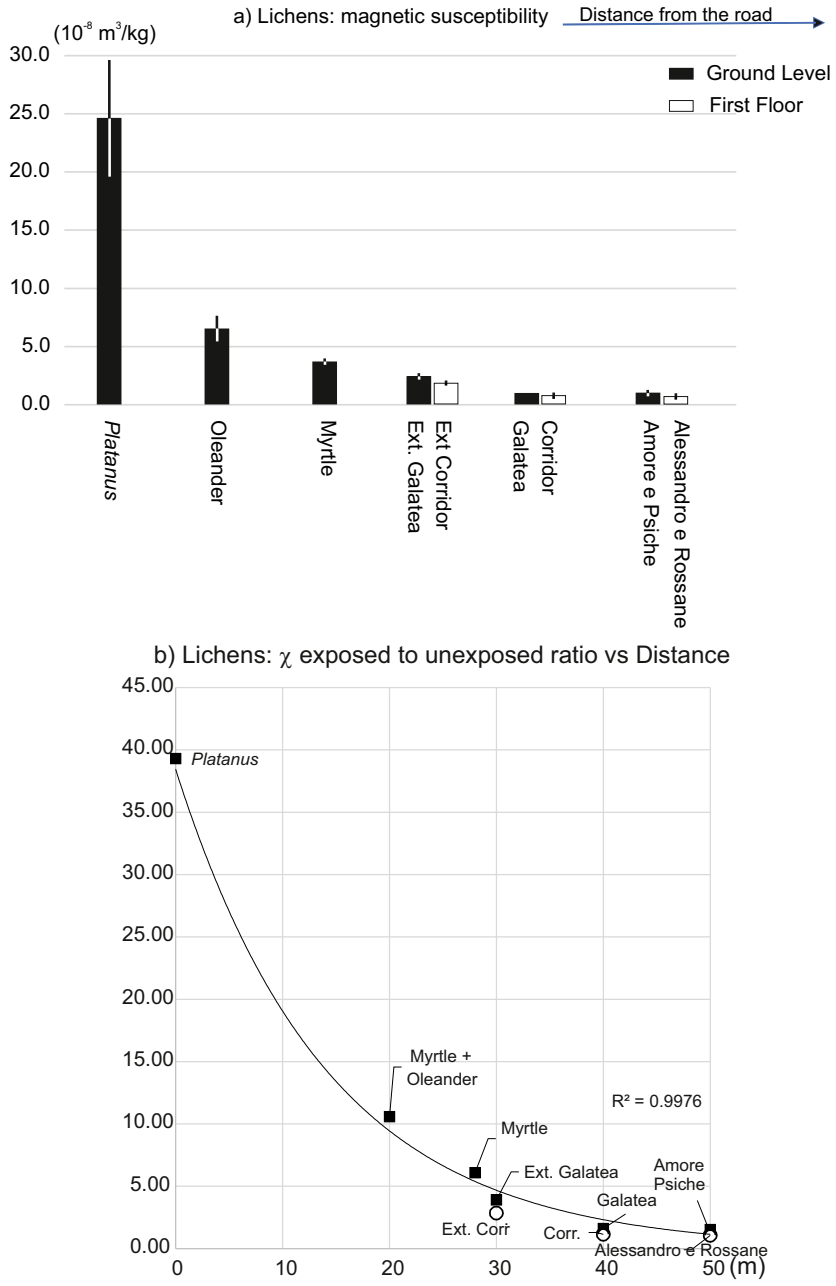


**Fig. 5.** The variability of lichens' magnetic susceptibility with the distance from the road: (a) average values and standard errors of mass magnetic susceptibility of lichens exposed for three months, black bars for samples on the ground floor, white for the first floor; (b) exponential decay of the magnetic susceptibility ($\chi$) ratio vs distance from the road, calculated as the magnetic susceptibility of exposed transplants normalized to the average value of the unexposed samples. Distances were evaluated by means of the proper Google Earth function, and successively verified through laser telemeter measurements.

Agrawal, 2018): Manes et al. (2016) estimated that urban green, in the Rome Metropolitan area, removed 1159.90 Mg of $PM_{10}$ in 2003.

### 4.2. Magnetic mineralogy of leaves and lichens

In general, for both lichens and leaves, the magnetic properties suggest that magnetite-like minerals are the main magnetic carriers, as confirmed by the SIRM/$\chi$ average values reported in Table 1 and Table 1s (Thompson and Oldfield, 1986).

For what concerns the domain state and the grain size of the magnetic particles, the role of the "Day plot" is under discussion for its intrinsic limitations (Roberts et al., 2018); nevertheless, it is used here as an empirical tool for comparison with previous studies addressed to the magnetism of traffic-related particulate matter. When compared with the average data obtained for fuel and brake emissions sampled in cars' exhaust pipes and wheel rims (Sagnotti et al., 2009), *Platanus* leaves and lichens are placed close to the "brake" data points (Fig. 3), consistently with magnetic biomonitoring surveys carried out on lichens transplanted in Milan and on tree leaves sampled in Rome, where multidisciplinary analyses pinpointed brake abrasion as the main source of urban PM (Winkler et al., 2020; Fusaro et al., 2021). Notably, the position in the diagram is slightly shifted, with respect to "pure" brake behavior, towards the central zone of the plot, similarly to the *Quercus Ilex* leaves investigated by Sagnotti et al. (2009), who did not exclude the influence of a secondary weaker magnetic component connected to fuel exhaust emissions. Moving away from the roadway and towards the Halls, the position of lichen transplants gradually migrated

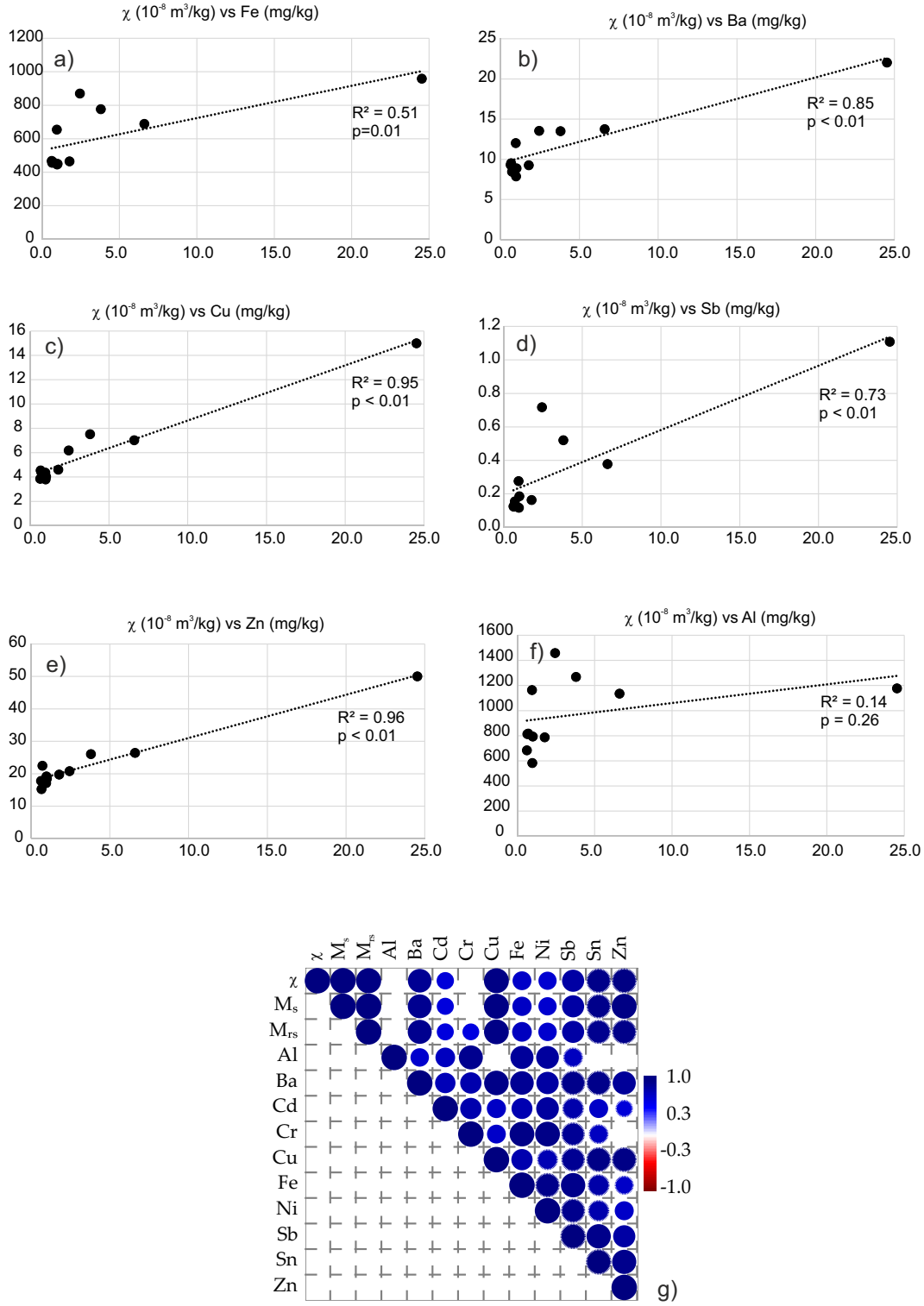


**Fig. 6.** Selected linear correlations between magnetic susceptibility ($\chi$) of lichens and element concentration (a, Fe; b, Ba, c, Cu; d, Sb; e, Zn; f, Al): all the elements but Al and Cr significantly correlated with $\chi$, at 95% confidence level. g) correlation plot of concentration dependent magnetic parameters and element concentration: the circle dimension represents the value of r, the linear correlation parameter, in blue when positive.

towards those occupied by control and soil samples, in the central-upper area of the plot, near the theoretical trends for natural magnetite, with a possible presence of magnetic particles related to fuel exhausts.

Magnetic measurements well discriminate brakes from other magnetic emissions, e. g. by means of the "Day plot", but fuel exhaust and fine natural magnetic components are somewhat difficult to be disentangled. In the "Day Plot", as already observed for the concentration-dependent magnetic parameters, lichens outlined better than leaves the gradual transition from outdoor traffic-related bioaccumulation to indoor apparently uncontaminated or very slightly contaminated conditions.

The SIRM/$\chi$ average value (6.7 ± 2.5 kA/m) for September leaves is in line with brakes as the main emissions (Chaparro et al., 2010;

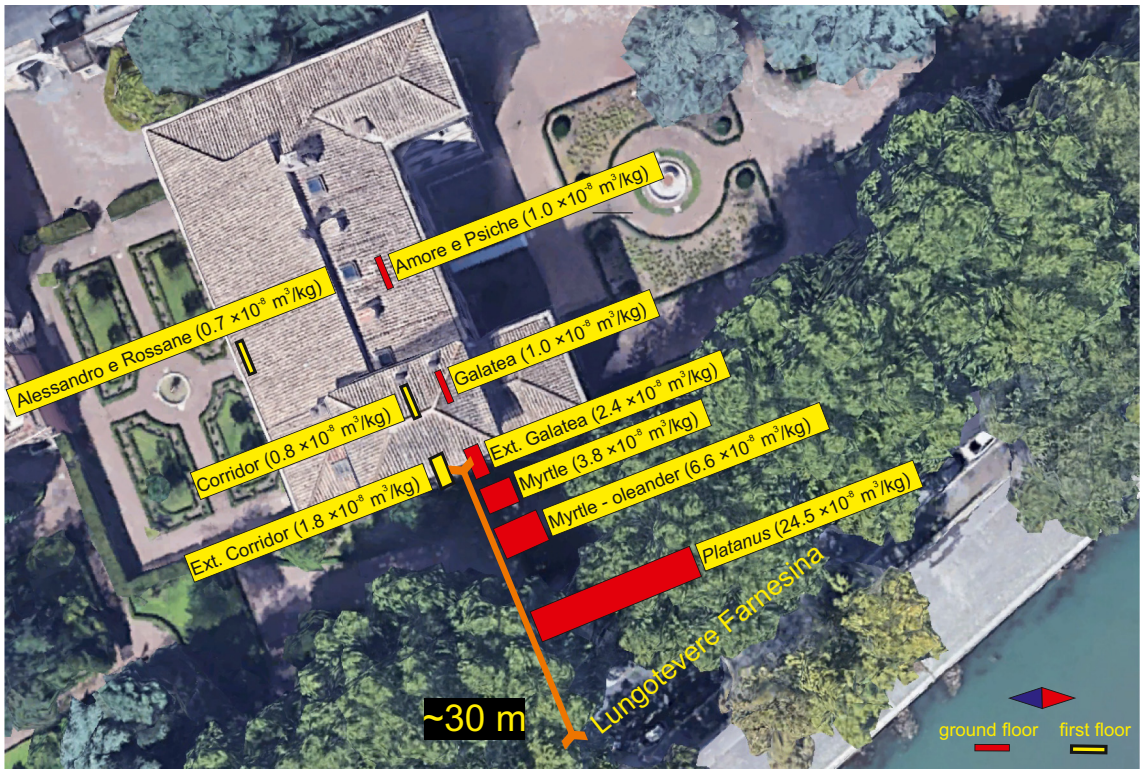


**Fig. 7.** Modified Google Earth aerial view of Villa Farnesina: the magnetic susceptibility values of lichen transplants are superimposed to the sampling sites as histograms. The magnetic susceptibility values decay with the distance from the road, that was evaluated by means of the proper Google Earth function and verified through the measurement with a laser telemeter.

Gonet and Maher, 2019), and distinct from gasoline and diesel exhausts (13.8 ± 6.3 kA/m and 14.5 ± 12.1 kA/m, respectively). For lichens, SIRM/$\chi$ values increase with distance from the road, gradually approaching the noticeably higher values carried by unexposed samples, that is, on average, 29 kA/m, a value that can be ascribed to finer natural magnetite grains. The large variability in SIRM/$\chi$ values in lichens far from the roadside is likely due to the worse determination of SIRM values on small gel caps of samples containing a low amount of magnetic particles.

The FORC diagrams of *Platanus* and cypress leaves (Fig. 4a, c) as well as roadside lichens (Fig. 4b) peaked at the origin of the diagrams, showing prevailing MD features and a sharp tail extending to higher coercivities, closely resembling those for brakes and leaves reported by Sagnotti et al. (2009) and Winkler et al. (2020), and in overall agreement with the considerations made after the "Day plot" and SIRM/$\chi$ values: brakes emissions dominate the magnetic properties of PM in outdoor samples close to the road. The sharp tail extending to higher coercivities on the FORC diagrams was recently attributed to nanoscale particles of metallic Fe arising from brake pads (Sheikh et al., 2022).

A single-domain magnetic component peaked, at around 20 mT, the noisier FORC distribution of a control sample (Fig. 4f), myrtle-oleander (Fig. 4d) and Amore e Psiche (Fig. 4e) lichen transplants, highlighting a weak and presumably natural magnetic component preexisting to the lichen exposure and emerging only when the contribution of brake emission is negligible.

This weak SD component might also be connected to the minor fuel exhaust contribution shifting the points of the roadside leaves on the "Day plot", with respect to "pure" brake behavior, as interpreted for *Q. ilex* leaves sampled in Rome (Sagnotti et al., 2009).

Moreover, it is expected that fine SD magnetic components are able to reach farther distances with respect to the coarser fraction of MD brakes emissions, thus appearing in the outdoor samples that are relatively far from the roadside. Overall, these results are compliant with Gonet et al. (2021a, 2021b), who concluded that non-exhaust vehicle brake wear is the major source of airborne magnetite in traffic-related contexts; they also estimated that, at the roadside of Lancaster and Birmingham, brake wear contributes 68–85% of the total airborne magnetite in the roadside environment, followed by diesel exhaust emissions (7–12%), petrol exhaust emissions (2–4%) and background dust (6–10%).

About the grain size of brake emissions, Gonet and Maher (2019) showed that Fe-bearing particles arise from the friction between a brake pad and the cast iron disc: at operating temperatures below 200 °C, abrasive processes dominate, and wear particles >1 μm are mostly generated. At higher temperatures (>190 °C), the concentration of nanoparticles (<100 nm) increases by 4–6 orders of magnitude and constitutes >90% of total brake dusts.

In this study, the magnetic properties that are diagnostic of the presence of SP particles—e.g., the enhancement of magnetic susceptibility, very low SIRM/k values, asymmetry along the $B_u$ axis in FORC diagrams— did not supported the presence of ultrafine magnetic particles.

Conversely, the position of the outdoor samples in the "Day plot" might depend on the coexistence of SP and MD granulometric fractions, as well as the fact that the chemically-impure composition of the magnetite-like particles prevent the points to fall near the zones and the mixing lines calculated for theoretical magnetite.

As a further difficulty, Muxworthy et al. (2003) and Sagnotti and Winkler (2012) showed that in traffic-related PM, the SP fraction may occur as coating of MD particles, being originated by localized stress in the oxidized outer shell surrounding the unoxidized core of magnetite-like grains: thus, it should not be considered as a direct proxy for the overall content of ultrafine <30 nm particles.

Conversely, Gonet et al. (2021b), demonstrated that most brake-wear particles are smaller than 200 nm, and that even the larger brake-wear PM size fractions are dominated by agglomerates of ultrafine grains.

Magnetic measurements well discriminate brakes from other magnetic emissions, but fuel exhausts and fine natural magnetic components are

somewhat difficult to be uncoupled; the association between the magnetic grain size and the domain state is not always straightforward and, for what concerns the harmful ultrafine magnetic particles, they are difficult to be investigated at standard room temperature for their unstable magnetic properties.

### 4.3. Comparison of magnetic and chemical properties of lichens and element deposition fluxes

Exhaust emissions constitute a substantial source of magnetic particles in urban environments, even if 90% of tailpipe emissions is carbonaceous material (Gonet and Maher, 2019). Trace elements emitted by engines include Fe, Zn, Cr, Mo, Ti, Mg, Ni, Pb, Ca, Cu, Ba, Sb, Co, Cd, V, Pt and Pd.

Brake wear debris comprises primarily carbonaceous and metal-bearing components but, in contrast to tailpipe emissions, Fe often dominates, constituting >50 wt% of all brake wear emissions: besides Fe, brake dust emissions include Cu, C, Ba, Sb, Si, Al, Mo, S, Sn, Cd, Cr, Pb, Zr, Ti and Zn (Gonet and Maher, 2019; Iijima et al., 2007).

Thus, the statistical associations between magnetic susceptibility and chemical elements corroborates the results of the magnetic analyses: the main source of particulate pollution is vehicular traffic, mostly from brake abrasion emissions.

A major soil contamination of lichen samples can be ruled out, considering that no significant correlation emerged between Al and magnetic properties.

The knowledge of element deposition fluxes is of paramount importance, especially in indoor environments, since chronic exposure to ambient PM is associated with a wide array of adverse effects for human health (Churg et al., 2003) and for cultural heritage (Comite et al., 2019; Grossi and Brimblecombe, 2004). However, this kind of data is rarely available, and the possibility offered by lichen biomonitoring techniques for such an estimation is invaluable. Estimated element deposition rates at the Lungotevere road and the Garden of Villa Farnesina are consistent with those estimated for Milan (Contardo et al., 2020) and those measured in other large cities such as Los Angeles (Sabin et al., 2006), Chicago (Shahin et al., 2000), Munich (Dietl et al., 1997), Paris (Ayrault et al., 2013), while estimated element deposition rates at indoor Halls are similar to those reported for background or lightly polluted environments (Schneider et al., 2021; Shelley et al., 2017), in strong agreement with the magnetic observations.

## 5. Conclusions

This study represents the first multidisciplinary biomonitoring approach for assessing the impact of vehicular traffic on cultural heritage located within trafficked urban contexts.

It was tested if the Halls of Villa Farnesina in Rome, frescoed, among others, by Raffaello Sanzio, are preserved from large inputs of vehicular magnetic particles, because of the distance from the roadside and the ecosystem services provided by trees and shrubs at the Lungotevere road and inside the gardens of the Villa.

The partial constraints for the containment of Covid-19 pandemic helped in the discrimination of natural and vehicular PM sources, disregarding the influence of the indoor activities connected to the visits by individuals, schools and large groups, which were not allowed for most of the time.

The main outcomes of this study are:

1) Plant leaves and transplanted lichens are very different but complementary biomonitors, and their combined use is desirable for applying these methodologies under distinct visions and perspectives.
   Leaves are widely distributed in urban contexts and are effective for an immediate and basic outline of particulate matter bioaccumulation, which strongly depends on the plant species and is preparatory for assessing the inter-species differences in providing phytoremediation and preventive conservation services. Lichen transplants constitute state of the art biomonitors, by means of chemical and magnetic properties measured after a determined period of exposure and compared to known initial conditions. Moreover, lichens can be used for planning outdoor vs indoor sampling designs, providing a chance for investigating the directional diffusion of airborne particulate matter inside the interiors of civil and historical buildings.
2) The magnetic and chemical properties of plant leaves and lichen transplants exposed around and inside Villa Farnesina depended on the bioaccumulation of traffic related magnetite-like particles associated, among others, to Cu, Ba and Sb, mainly emitted by vehicular brakes.
   The magnetic susceptibility of lichens decreased exponentially with the distance from the road: the frescoed Halls, over 30 m far from the roadway and protected by the trees, were preserved from significant inputs of traffic-related magnetic particles.

Magnetic biomonitoring demonstrated once more to be a fast, cheap and very sensitive methodology for outlining the impact of vehicular particulate emissions, suggesting its use for further investigations at cultural heritage sites located within complex metropolitan areas.

## CRediT authorship contribution statement

**Aldo Winkler:** Conceptualization, Methodology, Validation, Formal analysis, Investigation, Writing – original draft and revision, Visualization, Supervision, Funding acquisition. **Tania Contardo:** Conceptualization, Methodology, Validation, Formal analysis, Investigation, Writing – original draft, Visualization. **Virginia Lapenta:** Investigation, Supervision, Logistics. **Antonio Sgamellotti:** Conceptualization, Investigation, Supervision, Logistics. **Stefano Loppi:** Conceptualization, Methodology, Validation, Formal analysis, Investigation, Writing – original draft and revision, Visualization, Supervision.

## Declaration of competing interest

The authors declare that they have no known competing financial interests or personal relationships that could have appeared to influence the work reported in this paper.

## Acknowledgments

The magnetic analyses were supported by INGV Project “Pianeta Dinamico” (Ministry of University and Research, Task A3 – 2021, CUP D53J19000170001).

The Lakeshore 8604 VSM was funded by the Ministry of University and Research, project PON GRINT, code PIR01_00013.

AW thanks Fabrizia Buongiorno, Carlo Doglioni and Massimo Musacchio for the friendly and stimulating collaboration within the Pianeta Dinamico project. The Editors (Elena Paoletti and Jay Gan) and the reviewers are deeply thanked for the careful handling of the paper.

## Appendix A. Supplementary data

Supplementary data to this article can be found online at https://doi.org/10.1016/j.scitotenv.2022.153729.

## References

Ayrault, S., Rianti Priadi, C., Le Pape, P., Bonté, P., 2013. Occurrence, sources and pathways of antimony and silver in an urban catchment. In: De La Guardia, M., Armenta, S. (Eds.), The Quality of Air. Comprehensive Analytical Chemistry 73. Elsevier, Amsterdam, p. 425.

Bačkor, M., Loppi, S., 2009. Interactions of lichens with heavy metals. Biol. Plant. 53 (2), 214–222. https://doi.org/10.1007/s10535-009-0042-y.

Blanusa, T., Fantozzi, F., Monaci, F., Bargagli, R., 2015. Leaf trapping and retention of particles by holm oak and other common tree species in Mediterranean urban environments. Urban For. Urban Green. 14 (4), 1095–1101. https://doi.org/10.1016/j.ufug.2015.10.004.

Chaparro, M.A.E., Marié, D.C., Gogorza, C.S.G., Navas, A., Sinito, A.M., 2010. Magnetic studies and scanning electron microscopy – X-ray energy dispersive spectroscopy

analyses of road sediments, soils and vehicle-derived emissions. Stud. Geophys. Geod. 54, 633–650.
Churg, A., Brauer, M., del Carmen Avila-Casado, M., Fortoul, T.I., Wright, J.L., 2003. Chronic exposure to high levels of particulate air pollution and small airway remodeling. Environ. Health Perspect. 111, 5. https://doi.org/10.1289/ehp.6042.
Cislaghi, C., Nimis, P., 1997. Lichens, air pollution and lung cancer. Nature 387, 463–464. https://doi.org/10.1038/387463a0.
Comite, V., Pozo-Antonio, J.S., Cardell, C., Rivas, T., 2019. Metals distributions within black crusts sampled on the facade of an historical monument: The case study of the Cathedral of Monza (Milan, Italy). IMEKO TC4 International Conference on Metrology for Archaeology and Cultural Heritage, MetroArchaeo: 4 through 6 December. International Measurement Federation Secretariat (IMEKO), pp. 73–78.
Contardo, T., Giordani, P., Paoli, L., Vannini, A., Loppi, S., 2018. May lichen biomonitoring of air pollution be used for environmental justice assessment? A case study from an area of N Italy with a municipal solid waste incinerator. Environ. Forensic 19 (4), 265–276. https://doi.org/10.1080/15275922.2018.1519742.
Contardo, T., Vannini, A., Sharma, K., Giordani, P., Loppi, S., 2020. Disentangling sources of trace element air pollution in complex urban areas by lichen biomonitoring. A case study in Milan (Italy). Chemosphere 256, 127155.
Conti, M.E., Cecchetti, G., 2001. Biological monitoring: lichens as bioindicators of air pollution assessment—a review. Environ. Pollut. 114 (3), 471–492. https://doi.org/10.1016/S0269-7491(00)00224-4.
Day, R., Fuller, M., Schmidt, V.A., 1977. Hysteresis properties of titanomagnetites: grain-size and compositional dependence. Phys. Earth Planet. Inter. 13, 260–267. https://doi.org/10.1016/0031-9201(77)90108-X.
Dietl, C., Reifenhauser, W., Peicl, L., 1997. Association of antimony with traffic – occurrence in airborne dust, deposition and accumulation in standardized grass cultures. Sci. Total Environ. 205, 235–244.
Dunlop, D.J., 2002a. Theory and application of the day plot (MRS/MS versus HCR/HC) 1. Theoretical curves and tests using titanomagnetite data. J. Geophys. Res., 107. https://doi.org/10.1029/2001JB000487.
Dunlop, D.J., 2002b. Theory and application of the day plot (MRS/MS versus HCR/HC) 2. Application to data for rocks, sediments, and soils. J. Geophys. Res., 107. https://doi.org/10.1029/2001JB000486.
Flanders, P.J., 1994. Collection, measurement, and analysis of airborne magnetic particulates from pollution in the environment. J. Appl. Phys. 75 (10), 5931–5936. https://doi.org/10.1063/1.355518.
de la Fuente, D., Vega, J.M., Viejo, F., Díaz, I., Morcillo, M., 2013. Mapping air pollution effects on atmospheric degradation of cultural heritage. J. Cult. Herit. 14 (2), 138–145. https://doi.org/10.1016/j.culher.2012.05.002.
Fusaro, L., Marando, F., Sebastiani, A., Capotorti, G., Blasi, C., Copiz, R., Congedo, L., Munafò, M., Ciancarella, L., Manes, F., 2017. Mapping and assessment of PM10 and O3 removal by woody vegetation at urban and regional level. Remote Sens. 9, 791. https://doi.org/10.3390/rs9080791.
Fusaro, L., Salvatori, E., Winkler, A., Frezzini, M.A., De Santis, E., Sagnotti, L., Canepari, S., Manes, F., 2021. Urban trees for biomonitoring atmospheric particulate matter: an integrated approach combining plant functional traits, magnetic and chemical properties. Ecol. Indic. 126. https://doi.org/10.1016/j.ecolind.2021.107707.
Georgeaud, V.M., Rochette, P., Ambrosi, J.P., Vandamme, D., Williamson, D., 1997. Relationship between heavy metals and magnetic properties in a large polluted catchment: the etang de berre (south of France). Phys.Chem. Earth 22 (1–2), 211–214. https://doi.org/10.1016/S0079-1946(97)00105-5.
Gonet, T., Maher, B.A., 2019. Airborne, vehicle-derived fe-bearing nanoparticles in the urban environment—a review. Environ. Sci. Technol. 53, 9970–9991.
Gonet, T., Maher, B.A., Kukutschová, J., 2021. Source apportionment of magnetite particles in roadside airborne particulate matter. Sci.Total Environ. 752, 141828. https://doi.org/10.1016/j.scitotenv.2020.141828.
Gonet, T., Maher, B.A., Nyirő-Kósa, I., Pósfai, M., Vaculík, M., Kukutschová, J., 2021. Size-resolved, quantitative evaluation of the magnetic mineralogy of airborne brake-wear particulate emissions. Environ. Pollut. 288, 117808. https://doi.org/10.1016/j.envpol.2021.117808.
Grau-Bové, J., Strlič, M., 2013. Fine particulate matter in indoor cultural heritage: a literature review. HeritageScience 1 (1). https://doi.org/10.1186/2050-7445-1-8.
Grossi, C.M., Brimblecombe, P., 2004. Aesthetics of simulated soiling patterns on architecture. Environ. Sci. Technol. 38 (14), 3971–3976. https://doi.org/10.1021/es0353762.
Hackney, S., 1984. The distribution of gaseous air pollution within museums. Stud. Conserv. 29 (3), 105–116.
Hammer, Ø., Harper, D.A.T., Ryan, P.D., 2001. PAST: paleontological statistics software package for education and data analysis. Palaeontol. Electron. 4, 9.. http://palaeo-electronica.org/2001_1/past/issue1_01.htm.
Hansard, R., Maher, B.A., Kinnersley, R.P., 2012. Rapid magnetic biomonitoring and differentiation of atmospheric particulate pollutants at the roadside and around two major industrial sites in the U.K. Environ. Sci. Technol. 46, 4403–4410.
Harrison, R.J., Feinberg, J.M., 2008. FORCinel: an improved algorithm for calculating first-order reversal curve distributions using locally weighted regression smoothing. Geochem. Geophys. Geosyst. 9.
Hofman, J., Wuyts, K., Wittenberghe, S.Van, Samson, R., 2014. On the temporal variation of leaf magnetic parameters: seasonal accumulation of leaf-deposited and leaf-encapsulated particles of a roadside tree crown. Sci. Total Environ. 493, 766–772. https://doi.org/10.1016/j.scitotenv.2014.06.074.
Hofman, J., Staelens, J., Cordell, R., Stroobants, C., Zikova, N., Hama, S.M.L., Wyche, K.P., Kos, G.P.A., Van Der Zee, S., Smallbone, K.L., et al., 2016. Ultrafine particles in four european urban environments: results from a new continuous long-term monitoring network. Atmos. Environ. 136, 68–81. https://doi.org/10.1016/j.chemosphere.2020.127155.
Hofman, J., Maher, B.A., Muxworthy, A.R., Wuyts, K., Castanheiro, A., Samson, R., 2017. Biomagnetic monitoring of atmospheric pollution: a review of magnetic signatures from biological sensors. Environ. Sci. Technol. 51, 6648–6664.
Hunt, A., Jones, J., Oldfield, F., 1984. Magnetic measurements and heavy metals in atmospheric particulates of anthropogenic origin. Sci. Total Environ. 33, 129–139.
Iijima, I., Sato, K., Yano, K., Tago, H., Kato, M., Kimura, H., Furuta, N., 2007. Particle size and composition distribution analysis of automotive brake abrasion dust for the evaluation of antimony sources of airborne particulate matter. Atmos. Environ. 41, 4908–4919.
Kardel, F., Wuyts, K., Maher, B.A., Samson, R., 2012. Intra-urban spatial variation of magnetic particles: monitoring via leaf saturation isothermal remanent magnetisation (SIRM). Atmos. Environ. 55, 111–120.
Lambert, S., 2010. Italy and the history of preventive conservation. NovemberCeROArt. Conservation, Exposition, Restauration d'Objets d'Art (No. EGG 1). Association CeROArt asbl. https://doi.org/10.4000/ceroart.1707.
Loppi, S., 2014. Lichens as sentinels for air pollution at remote alpine areas (Italy). Environ. Sci. Pollut. Res. 21 (4), 2563–2571.
Loppi, S., 2019. May the diversity of epiphytic lichens be used in environmental forensics? Diversity 11 (3), 36.
Loppi, S., Paoli, L., 2015. Comparison of the trace element content in transplants of the lichen Evernia prunastri and in bulk atmospheric deposition: a case study from a low polluted environment (C Italy). Biologia 70 (4), 460–466.
Loppi, S., Pirintsos, S.A., 2003. Epiphytic lichens as sentinels for heavy metal pollution at forest ecosystems (central Italy). Environ. Pollut. 121 (3), 327–332.
Loppi, S., Ravera, S., Paoli, L., 2019. Coping with uncertainty in the assessment of atmospheric pollution with lichen transplants. Environ. Forensic 20 (3), 228–233.
Maher, B.A., Moore, C., Matzka, J., 2008. Spatial variation in vehicle-derived metal pollution identified by magnetic and elemental analysis of roadside tree leaves. Atmos. Environ. 42, 364–373.
Manes, F., Marando, F., Capotorti, G., Blasi, C., Salvatori, E., Fusaro, L., Ciancarella, L., Mircea, M., Marchetti, M., Chirici, C., Munafò, M., 2016. Regulating ecosystem services of forests in ten italian metropolitan cities: air quality improvement by PM10 and O3 removal. Ecol. Ind. 67, 425–440. https://doi.org/10.1016/j.ecolind.2016.03.009.
Marié, D.C., Chaparro, M.A.E., Irurzun, M.A., Lavornia, J.M., Marinelli, C., Cepeda, R., Böhnel, H.N., Castañeda Miranda, A.G., Sinito, A.M., 2016. Magnetic mapping of air pollution in Tandil city (Argentina) using the lichen parmotrema pilosum as biomonitor. Atmos. Pollut. Res. 7, 513–520.
Matzka, J., Maher, B.A., 1999. Magnetic biomonitoring of roadside tree leaves: identification of spatial and temporal variations in vehiclederived particulates. Atmos. Environ. 33, 4565–4569.
McIntosh, G., Gómez-Paccard, M., Osete, M.L., 2007. The magnetic properties of particles deposited on Platanus x hispanica leaves in Madrid, Spain, and their temporal and spatial variations. Sci. Total Environ. 382, 135–146.
Moreno, E., Sagnotti, L., Dinarès-Turell, J., Winkler, A., Cascella, A., 2003. Biomonitoring of traffic air pollution in Rome using magnetic properties of tree leaves. Atmos. Environ. 37, 2967–2977.
Muhammad, S., Wuyts, K., Samson, R., R., 2019. Atmospheric net particle accumulation on 96 plant species with contrasting morphological and anatomical leaf characteristics in a common garden experiment. Atmos. Environ. 202, 328–344. https://doi.org/10.1016/j.atmosenv.2019.01.015.
Muhammad, S., Wuyts, K., Samson, R., 2020. Immobilized atmospheric particulate matter on leaves of 96 urban plant species. Environ. Sci. Pollut. Res. 27 (29), 36920–36938. https://doi.org/10.1007/s11356-020-09246-6.
Mukherjee, A., Agrawal, M., 2018. Air pollutant levels are 12 times higher than guidelines in Varanasi, India. Sources and transfer. Environmental Chemistry Letters 16 (3), 1009–1016.
Muxworthy, A.R., Matzka, J., Fernández Davila, A., Petersen, N., 2003. Magnetic signature of daily sampled urban atmospheric particles. Atmos. Environ. 37 (29), 4163–4169. https://doi.org/10.1016/S1352-2310(03)00500-4.
Paoli, L., Fačkovcová, Z., Guttová, A., Maccelli, C., Kresáňová, K., Loppi, S., 2019.. Evernia goes to school: bioaccumulation of heavy metals and photosynthetic performance in lichen transplants exposed indoors and outdoors in public and private environments. Plants 8 (5), 125.
Paoli, L., Maccelli, C., Guarnieri, M., Vannini, A., Loppi, S., 2019.. Lichens "travelling" in smokers' cars are suitable biomonitors of indoor air quality. Ecol. Indic. 103, 576–580.
Pike, C.R., Roberts, A.P., Verosub, K.L., 1999. Characterizing interactions in fine magnetic particle systems using first order reversal curves. J. Appl. Phys. 85, 6660–6667.
Qian, J., Ferro, A.R., Fowler, K.R., 2008. Estimating the resuspension rate and residence time of indoor particles. J. Air Waste Manag. Assoc. 58 (4), 502–516. https://doi.org/10.3155/1047-3289.58.4.502.
Roberts, A., Pike, C.R., Verosub, K.L., 2000. First-order reversal curve diagrams: a new tool for characterizing the magnetic properties of natural samples. J. Geophys. Res. 105, 28461–28475.
Roberts, A.P., Tauxe, L., Heslop, D., Zhao, X., Jiang, Z., 2018. A critical appraisal of the "day" diagram. J. Geophys. Res. Solid Earth 123, 2618–2644. https://doi.org/10.1002/2017JB015247.
Sabin, L.D., Lim, J.H., Stolzenbach, K.D., Schiff, K.C., 2006. Atmospheric dry deposition of trace metals in the coastal region of Los Angeles, California, USA. Environ. Toxicol. Chem. 25 (9), 2334–2341.
Sagnotti, L., Taddeucci, J., Winkler, A., Cavallo, A., 2009. Compositional, morphological, and hysteresis characterization of magnetic airborne particulate matter in Rome, Italy geochem. Geophys. Geosyst. 10 (8). https://doi.org/10.1029/2009GC002563.
Sagnotti, L., Winkler, A., 2012. On the magnetic characterization and quantification of the superparamagnetic fraction of traffic-related urban airborne PM in Rome, Italy. Atmos. Environ. 59, 131–140. https://doi.org/10.1016/j.atmosenv.2012.04.058.
Salo, H., Paturi, P., Mäkinen, J., 2016. Moss bag (Sphagnum papillosum) magnetic and elemental properties for characterising seasonal and spatial variation in urban pollution. Int. J. Environ. Sci. Technol. 13, 1515–1524.

Schneider, T., Musa Bandowe, B.A., Bigalke, M., Mestrot, A., Hampel, H., Mosquera, P.V., Fränkl, L., Wienhues, G., Vogel, H., Tylmann, W., Grosjean, M., 2021. 250-Year records of mercury and trace element deposition in two lakes from Cajas National Park, SW Ecuadorian Andes. Environ Sci. Pollut Res Int. 28 (13), 16227–16243. https://doi.org/10.1007/s11356-020-11437-0 Epub 2020 Dec 5.

Shahin, U., Yi, S.M., Paode, R.D., Holsen, T.M., 2000. Long-term elemental dry deposition fluxes measured around Lake Michigan with an automated dry deposition sampler. Environ. Sci. Technol. 34, 1887–1895.

Sheikh, H.A., Maher, B.A., Karloukovski, V., Lampronti, G.I., Harrison, R.J., 2022. Biomagnetic characterization of air pollution particulates in Lahore, Pakistan. Geochem. Geophys. Geosystems 23, e2021GC010293. https://doi.org/10.1029/2021GC010293.

Shelley, R.U., Roca-Martí, M., Castrillejo, M., Sanial, V., Masqué, P., Landing, W.M., Planquette, H., Sarthou, G., 2017. Quantification of trace element atmospheric deposition fluxes to the Atlantic Ocean (>40°N; GEOVIDE, GEOTRACES GA01) during spring 2014. Deep. Res. I (119), 34–49. https://doi.org/10.1016/j.dsr.2016.11.010.

Szönyi, M., Sagnotti, L., Hirt, A.M., 2008. A refined biomonitoring study of airborne particulate matter pollution in Rome, with magnetic measurements on quercus ilex tree leaves. Geophys. J. Int. 173, 127–141. https://doi.org/10.1111/j.1365-246X.2008.03715.x.

Thompson, R., Oldfield, F., 1986. Magnetic properties of natural materials. Environmental Magnetism. Springer, Dordrecht, pp. 21–38.

Uring, P., Chabas, A., Alfaro, S., Derbez, M., 2020. Assessment of indoor air quality for a better preventive conservation of some french museums and monuments. Environ. Sci. Pollut. Res. 27 (34), 42850–42867. https://doi.org/10.1007/s11356-020-10257-6.

Winkler, A., Contardo, T., Vannini, A., Sorbo, S., Basile, A., Loppi, S., 2020. Magnetic emissions from brake wear are the major source of airborne particulate matter bioaccumulated by lichens exposed in Milan (Italy). Appl. Sci. 10, 2073. https://doi.org/10.3390/app10062073.

Winkler, A., Amoroso, A., Di Giosa, A., Marchegiani, G., 2021. The effect of Covid- lockdown on airborne particulate matter in Rome, Italy: a magnetic point of view. Environmental Pollution 291, 118191. https://doi.org/10.1016/j.envpol.2021.11819 ISSN 0269.

Wolterbeek, H.T., Bode, P., 1995. Strategies in sampling and sample handling in the context of large-scale plant biomonitoring surveys of trace element air pollution. Sci. Total Environ. 176 (1–3), 33–43.